

# MEASUREMENT OF THE VELOCITY FIELD AND VOID FRACTION IN A PLANAR PLUNGING JET

F. Bonetto, R.T. Lahey, Jr.
*Center for Multiphase Research*
Rensselaer Polytechnic Institute
Troy, NY 12180-3590 USA



## ABSTRACT

This paper presents experimental data for a planar plunging liquid jet. Local data, including the void fraction, and the mean and turbulent bubble and liquid velocities were obtained using an impedance probe and a Laser Doppler Anemometer (LDA) - Fiber optics Laser Doppler Anemometer (FPDA) system. A dual element conductivity probe was also used to measure the spatial distribution of the local void fraction. The turbulence of the plunging jet was parametrically controlled using a special designed nozzle.

## INTRODUCTION





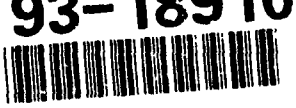

A good understanding of the air carryunder and bubble dispersion process associated with a plunging liquid jet is vital if one is to be able to quantify such diverse phenomena as breaking bow waves on surface ships, the meteorological significance of ocean waves, the performance of certain type of chemical reactors, the "greenhouse" effect (ie, the absorption of $CO_2$ by the oceans), and a number of other important maritime-related applications. The absorption of greenhouse gases

into the ocean has been hypothesized to be highly dependent upon the air carryunder that occurs due to breaking waves. This process can be approximated with a plunging liquid jet [Monahan, 1991], [Kerman, 1984]. In addition, the air entrainment process due to the breaking bow waves of surface ships may cause long (ie, up to 5 km in length) wakes. Naturally easily detectable wakes are undesirable for naval warships. The air carryunder that occurs at most hydraulic structures in rivers is also responsible for the large air/water mass transfer that is associated with these structures [Avery and Novak 1978]. Finally, air entrainment plays an important role in slug flow. The liquid film surrounding a rising Taylor bubble has a mean flow in the opposite direction from the Taylor bubble. This draining liquid film forms a plunging jet.. When this annular liquid jet exceeds a critical velocity Helmholtz instability occurs and the plunging liquid jet entrains small bubbles from the air in the Taylor bubble. These bubbles follow the Taylor bubble in the liquid slug and may coalesce with it. When gas entrainment exceeds coalescence a flow regime transition may occur.

A number of prior studies have been performed in which axisymmetric plunging jets have been used to investigate the air carryunder process. These include the work of Lin & Donnelly [1966], Burgess et al [1972], Van De Sande & Smith [1973], Koga [1982], McKeogh & Ervine [1981], Detsch & Sharma [1991], Ohkawa et al [1986] Ervine et al [1980], McKeogh & Elsaway [1980], Ervine & Falvey [1987], Blanchard & Cipriano [1981], Sene [1988] and Bonetto & Lahey [1993].

Unfortunately, in most of these experiments only global measurements were made (the notable exceptions being the work of McKeogh & Ervine [1981] and Bonetto & Lahey [1993]). While such measurements may allow one to correlate a

gross onset-of-air-carryunder criteria, they provide very limited information on the fluid mechanics of bubble entrainment and the resultant dispersion process in the induced two-phase jet.

These studies were done using a axisymmetric plunging jet. However many applications more closely resemble a planar plunging jet. Examples of applications that are better simulated with a planar jet are breaking ocean waves, the breaking bow waves of surface ships, the hydraulic structures in rivers and the draining liquid film around Taylor bubbles. This paper presents detailed data on a planar plunging liquid jet.

The primary objective of this research was to obtain detailed local data in the two-phase flow region of a planar plunging liquid jet. We have obtained the local velocities of the liquid and the gas bubbles, and the local void fraction of the. The probability density function of the bubble velocity was also measured, this is needed to estimate the total time that the bubbles remain submerged and therefore the total time that the bubbles are able to transfer mass. Similarly, the liquid turbulence intensity was measured since it is needed to compute interfacial mass transfer characteristics.



## EXPERIMENTAL APPARATUS

Figure-1 shows a schematic of the test section. A special screw pump was used to force the water through the nozzle.. The pump had a speed controller which was used to make the coarse control of the liquid flow rate through the nozzle. A bypass valve was used for the fine control of the liquid flow rate. In

order to damp out any flow oscillations, an accumulator was placed on the discharge side of the pump.

The acrylic planar nozzle, shown schematically in Figure-1, consisted of an arrangement of honeycombs and screens followed by a smooth contraction. In this way the turbulence level of the liquid jet could be parametrically varied. The exit width of the nozzle was 4.1 mm, and this produced a liquid jet of about the same width. Figure-1 also shows a nozzle bottom view and the dimensions of the slit. The acrylic tank which contained the water pool had dimensions, 0.914m x 0.916m x 1.465m = 1.265 $m^3$. The pump suction from the tank was put as far from the liquid jet impact point as possible in order to minimize the influence of the suction flow on the two-phase jet's flow.

A DANTEC Fiber-Flow Laser Doppler Anemometer (LDA) system was used to non intrusively measure the liquid and gas velocities (both the mean and fluctuations). This system consisted of submersible transmitting and receiving optics.

The transmitting optics were powered by a 10 W Ar-ion laser. The laser beam was split into two beams, where one beam passed through a Bragg cell to produce a fringe shift of 40 MHz in the measurement volume. Optical fiber wave guides conducted the laser beams to the submersible LDA heads. A 600 mm focal length lens was used in these experiments. A special beam expander was also used to reduce the size of the measurement volume and increase the light intensity.

The receiving optics was used in a back-scattering configuration. Optical fibers conducted the scattered light to the photomultipliers after the light was

optically filtered. The photomultipliers converted the optical signal into an electrical signal that was processed by a special covariance signal processor. An AT micro-computer then collected and processed the data.

The axial velocity of the liquid jet was used as the master signal for data collection. The signals collected by the AT computer consisted of the: (1)arrival time of the particles, (2) transit time of the particles, (3) velocity of the particles

An KfK dual element impedance probe was used to measure the local void fraction ($\alpha$). The impedance probe consists of two electrically isolated electrodes; one at the tip of the probe and another downstream electrode which was always in contact with the liquid in the pool. The liquid (ie, water) had a relatively high electrical conductivity and thus when the tip was in contact with the liquid a relatively high current flowed through to a Wheatstone bridge circuit. The difference between the conductivities of the liquid and gas phases produces a different signal depending on whether there is liquid or gas present at the tip of the probe. The active element of the probe's tip was 150$\mu$m in diameter and it was used to measure bubbles having diameters in the 2-4 mm range. This type of impedance probe is a standard tool used for measuring local void fraction in air/water bubbly flows [Hewitt, 1978].

The LDA/FPDA system and the KfK impedance probe were mounted on a Benjamin Systems three-dimensional traversing mechanism having a 1 $\mu$m positioning resolution. The tip of the KfK impedance probe was positioned 0.3 mm under the measurement volume of the LDA/FPDA system for void fraction measurements.

## EXPERIMENTAL RESULTS

The nozzle was oriented vertically producing an approximately rectangular liquid jet (4.1 mm x 75 mm). As shown in Figure-1 the rectangular slit was ended with a 4.1 mm in diameter semi-circumference in both edges. Nevertheless, the jet will be referred as a planar jet because of its large aspect ratio ($x_0/y_0$ =18). We observed that for low jet velocity a surface depression was produced near the perimeter of the jet. However, no air was entrained. When a threshold velocity was exceeded, it was observed that the plunging jet caused significant air entrainment.

We designed the nozzle in order to have the flexibility of setting up different configurations of honeycombs and grids. We found that the best configuration to minimize the turbulence intensity of the jet was to put an array of plastic straws at the nozzle entrance (i.e., upstream from the diffuser) to straighten the flow. We also put a honeycomb (circular cells, 3.1 mm in diameter) immediately downstream of the diffuser. With this set up the minimum turbulence intensity was 1.7% at the nozzle exit.

In a previous study Bonetto & Lahey, [1993] showed that the size of the entrained bubbles was a strong function of the plunging liquid jet's turbulence intensity for an axisymmetrical jet. Indeed, It was found that for a liquid jet with a low turbulence intensity (0.8%) the bubbles had an average diameter of about 200 μm. In contrast, a liquid jet with a turbulence intensity of 3% produced bubbles in the 2-4 mm range. The behavior of the planar jet used in this study was significantly different. In particular, we did not observe any appreciable effect of liquid jet turbulence intensity on the bubble size, and for all turbulence intensities studied the bubble size was in the 2-4 mm range. One possible reason is that the

influence of the jet's turbulence intensity on bubble size occurs at lower turbulent intensities than in the axisymmetric jet. Therefore we did not observe this effect because of our 1.7 % lower limit in turbulence intensity.

## VELOCITY RESULTS

The FPDA/LDA system was focused on the centerline of the jet at various distances (z) from the undisturbed free surface of the pool. The measurement volume was a prolate ellipsoid with a major axis of 1 mm and a minor axis of 0.1 mm. The liquid jet's flow rate was w = 1.8 kg/s. The FPDA system detected both the bubbles and the liquid seeding particles. The FPDA measurements were used to sort which particles were bubbles and which particles were liquid seeding as explained in previous work [Bonetto & Lahey, 1993]. Figure-2 shows the probability density function for the axial liquid velocity component corresponding to the jet's centerline (x = 0 mm, y = 0 mm, z = 31 mm). We see that the PDF has a Gaussian-like shape. The mean velocity (i.e., the zero order moment) of this PDF was $v_{lz} = 4.54$ m/s.

The first order moment of the distribution shown in Figure-2 (i.e., the rms fluctuation) is defined as,

$$\overline{v'_{lz}} = \frac{1}{n-1}\sqrt{\sum_{i=1}^{n}(V_{ilz} - \overline{V_{lz}})^2} \qquad (1)$$

The value of $\overline{v'_{lz}}$ in Figure-2 was 1.76 m/s. It is interesting to compare this value with the single-phase flow value for the same position and for the same liquid jet

flow rate. This single-phase flow value indicates the strength of the shear induced turbulence. Comparing both the single-phase value with the two-phase value we get a quantitative indication of the effect of bubble-induced turbulence. We see that the bubble-induced turbulence accounts for about 30% of the measured turbulence.

Figure-3 depicts the histogram of the gas velocity for the same conditions as Figure-2. There is a significant difference between the mean values of the liquid velocity and the gas velocity. The mean gas value was $v_{gz}$ = 4.15 m/s. The slip ratio was in this case $S=v_{gz}/v_{lz}$ =0.9. The corresponding rms fluctuation of the bubble velocity was $\overline{v'_{gz}}$ = 1.21 m/s. However the interpretation of this value is not as straightforward as in the liquid-phase case. For the liquid the rms fluctuation had two components. One was the turbulence produced by shear, the other was the bubble-induced pseudo-turbulence produced by the relative motion between the liquid and the bubbles. Both components contribute to the enhancement of mass or heat transfer between phases. The underlying physics behind the rms fluctuation of the gas velocity is different. There are two mechanisms that contributed to the rms fluctuation of the gas velocities. One is that due to the momentum exchange between the turbulent liquid eddies and the bubbles, the other is that we had a distribution of bubble sizes present. Therefore, even with an stagnant liquid and with bubbles moving in vertical straight lines, an Eulerian observer would record fluctuations in the bubble velocities due to different terminal rise velocities (produced by the different bubble sizes).

Figure-4 presents the liquid and gas phase mean velocities as a function of the lateral position (y) for a distance between the nozzle exit and the undisturbed pool level of h = 8.5 mm, a liquid jet flow rate of, w = 1.8 kg/s, and submergence

of, z = 31 mm. We see that at the centerline the relative velocity is $v_{rz}=v_{gz}-v_{lz}$ = 0.28 m/s. This is very close to the terminal velocity in water of a gas bubble having a 3 mm diameter. An ensemble average Two-Fluid model [Drew & Lahey, 1987] predicts that at a symmetry plane (where all lateral velocity gradients are zero due to symmetry) the relative velocity in the axial direction is determined by a balance between buoyancy and drag (i.e. the same forces that determines the terminal velocity). Our experimental finding support this conclusion.

We see Figure-4 that at the edge of the spreading two-phase jet that the gas (bubble ) velocity is negative, indicating buoyancy-driven countercurrent flow. It was also found that the two-phase jet was more dispersed than the corresponding single-phase flow case. This is presumably due to the fact that the presence of the gas phase obstructs a fraction of the flow area for the liquid producing an additional acceleration of the liquid and therefore a larger momentum interchange with the pool liquid. We also observed that the turbulence intensity was higher than in the single-phase flow due to bubble induced pseudoturbulence.

Figure-5 shows the liquid mean velocity for three different axial positions as a function of the lateral position (y) for w = 1.8 kg/s, h = 8.5 mm and x = 0 mm. The flat profile for z=1mm is characteristic of the potential flow which exited from the nozzle. Figure-5b-c also shows that the liquid velocity curves have a maximum at the centerline for all z. One can easily see from the figure how the liquid jet is spreading.

Figure-6 shows the corresponding bubble velocities profile at z=60.4 mm and z=90.4 mm. The bubble dispersion process is clearly evident.

## VOID FRACTION RESULTS

The local volume fraction, $\alpha$, is defined as the time fraction during which gas is present at the impedance probe's tip:

$$\alpha = \frac{\sum_{i=1}^{N} t_i}{T} \qquad (2)$$

The voltage signal from the KfK probe was used for these void fraction measurements. The voltage signal was post-processed using an algorithm based on voltage value thresholding and on the time derivative of the voltage signal, to minimize bubble detection errors. The measurement device was calibrated and the experimental error was approximately 0.01 (i.e., $\Delta\alpha = \pm 0.01$).

We tested the symmetry of the experimental setup and measurement system. Figure-7 shows the gas volume fraction as a function of lateral position (y)with the impedance probe tip z = 1 mm under the undisturbed pool surface. We notice that the void fraction was symmetric within the experimental error ($\Delta\alpha = \pm$ 0.01). This was a demanding test because of the strong gradients present at this axial location. Similar symmetry tests were conducted at different z locations with similar results.

Before discharging the loop and after each refill of the test loop with fresh water void fraction and velocity profiles were measured for conditions which were established as a benchmark. The reproducibility was inside the experimental error

reported previously which indicates that the effect of any changes due to surface tension variation were too small to be detected.

When the liquid jet impacts the pool surface, air entrainment occurs around the jet's circumference. As we move downward the bubbles are dispersed with a divergence angle. Figure-8 shows the void fraction as a function of the lateral position (y) for three different axial location (z). The spreading of the dispersed phase (i.e., the bubbles) can be easily seen in these plots. Figure-8 shows the case for z = 1 mm (i.e., the probe very close to the pool surface) where one can see a void fraction peak at about y = 3.5 mm. This peak is close to the liquid jet's edge (y = 2.05 mm) and most of the air is entrained in the peak neigborhood. For y = 0 mm (the centerplane) at z=1mm the void fraction had a minimum. This point corresponds to the liquid jet's center impacting the probe and therefore the bubbles population there is very small since little lateral dispersion had occurred. Figure-8 also shows how the void fraction peak off the centerline is reduced as we move down into the pool and also shows significant void dispersion as we move down into the pool. If we again consider the void fraction at the centerline (y = 0 mm) we see in Figure-9 a that $\alpha$ is negligible at z=0mm. As we move down into the pool spreading of the two-phase jet produces a void fraction build up at the centerline.

## SUMMARY & CONCLUSIONS

Detailed measurements were taken of the three-dimensional void fraction and fluid velocity fields beneath a plunging liquid jet. In particular, detailed LDA/FPDA data have been taken of the air dispersion process associated with a plunging planar liquid jet.

The bubbles entrained by the planar turbulent liquid jet had a mean diameter of about 3 mm, and the slip ratio was close to calculated values based on the terminal rise velocity of a single bubble. Moreover, the turbulence intensity of the spreading two-phase jet had two components, one due to shear-induced turbulence and the other due to bubble-induced pseudo-turbulence. Both components of turbulence were of the same order of magnitude.

These data provide the insights necessary for the development of analytical models of the air entrainment process. Moreover, they should also be useful for benchmarking phenomenological or mechanistic Computational Fluid Dynamic (CFD) analysis of the dispersion process in the induced two-phase jet.

## ACKNOWLEDGMENT

The financial support of this study by the Office of Naval Research (ONR) Grant No. N-0001491-J-1271 of the ONR Fluid Dynamics Program-1132F is gratefully acknowledged.

## REFERENCES

Avery, S. & Novak, P., "Oxygen Transfer at Hydraulic Structures," Journal of Hyd. Div., ASCE, Vol. 104(HY11, pp. 1521-1540 (1978).

Blanchard, D. and Cipriano, R., "Bubble and Aerosol Spectra Produced by a Laboratory Breaking Wave," J. Geophys. Res., Vol. 86c, p._8085, 1981.

Bonetto, F. & Lahey, R.T. Jr., "An Experimental Study on Air Carryunder due to a Plunging Liquid Jet " Int. J. Multiphase Flow, 19, No. 2, pp 281-294, 1993

Burgess, J.M., Molloy, N.A. and McCarthy, M.J., "A Note on the Plunging Liquid Jet Reactor," Chem. Eng. Sci., Vol. 12, 442, 1972.

Detsch, R. and Sharma, R.N., "The Critical Angle for Gas Bubble Entrainment by Plunging Liquid Jets," Chem. Eng. J., Vol. 44, pp. 157-166, 1990.

Drew, D., Lahey, R.T. Jr., "Application of General Constitutive Principles to the Derivation of Multidimensional Two-Phase Flow Equations," Int. J. Multiphase Flow, Vol. 5, pp. 243-264.

Dryden, H.L. and Schuabauen, G., "The Use of Damping Screens for the Reduction of Wind Tunnel Turbulence," JAS, 14, pp. 221-228, April 1947.

Durst, F., Eliasson, B., "Properties of Laser Doppler Signals and Their Exploitation for Particle Size Measurements," Proc. LDA Symp., Copenhagen, 1975, pp. 115-137.

Ervine, D.A., McKeogh, F. and Elsaway, E., "Effect of Turbulence Intensity on the Rate of Entrainment by Plunging Water Jets," Proc. of the Institute of Civil Engineers, Vol. 69, Part 2, pp. 425-445, 1980.

Ervine, D.A. and Falvey, H., "Behavior of Turbulent Water Jets in the Atmosphere and in Plunging Pools," Proc. Inst. Civil Engrs., Vol. 83, Part 2, pp. 295-314, 1987.

Groth, J. and Johansson, A., "Turbulence Reduction by Screens," J. Fluid Mechanics, Vol. 197, pp. 139-159, 1988.

Hewitt, G.B., Measurement of Two-Phase Parameters, Academic Press, 1978.

Kerman, B.R., "A Model of Interfacial Gas Transfer for a Well-Roughened Sea," Journal of Geophysical Research, Vol. 89(D1), pp. 1439-1446, 1984.

Koga, M., "Bubble Entrainment in Breaking Wind Waves," Tellus, Vol. 34, 481, 1982.

Lin, T.J. and Donnelly, H.G., "Gas Bubble Entrainment by Plunging Laminar Liquid Jets," AIChE Journal, Vol. 12, No. 3, 563, 1966.

McKeogh, E.J. and Elsaway, E., "Air Retained in Pool by Plunging Water Jet," J. of Hyd. Div., ASCE, 106(HY10), pp. 1577-1593, 1980.

McKeogh, E.J. and Ervine, D.A., "Air Entrainment Rate and Diffusion Pattern of Plunging Liquid Jets," Chem. Eng. Sci.. Vol. 36, 1161, 1981.

Monahan, L. and Torgersen, T., in Air Water Mass Transfer, edited by S. Wilhelms and J. Gulliver, American Society of Civil Engineers, 1991.

Moral, T., "Design of Two-Dimensional Wind Tunnel Contractions," J. Fluids Eng., pp. 371-378, 1977.

Ohkawa, A., Kusabinski, D., Kawai, Y., Sakai, N. and Endoh, K., "Some Flow Characteristics of a Vertical Liquid Jet System Having Downcomers," Chem. Eng. Sci., Vol. 51, pp. 2347-2361, 1986.

Prandtl, L., "Attaining a Steady Air Stream in Wind Tunnels," NACA TM 726, October 1933.

Rae, W. and Pope, A., Low Speed Wind Tunnel Testing, 2nd Ed., Wiley-Interscience, 1984.

Saffman, M., Buchhave, P. and Tanger, A., "Simultaneous Measurement of Size, Concentration and Velocity of Spherical Particles by a Laser Doppler Method," Proceedings of the Second International Symposium on Applications of Laser Anemometry to Fluid Mechanics, Lisbon, 1984.

Sene, K., "Air Entrainment by Plunging Jets," Chem. Eng. Sci., Vol. 43, p. 2615, 1988.

Scheiman, J. and Brooks. J.D., "Comparison of Experimental and Theoretical Turbulence Reduction from Screens, Honeycombs, and Honeycomb-Screen Combinations," JAS, 18, 638-643, August 1981.

Van De Sande, E. and Smith, J.M., "Surface Entrainment of Air by High Velocity Water Jets," Chem. Eng. Sci., Vol. 28, 1161, 1973.

**Figures**

**Figure-1: Schematics of the test section.**

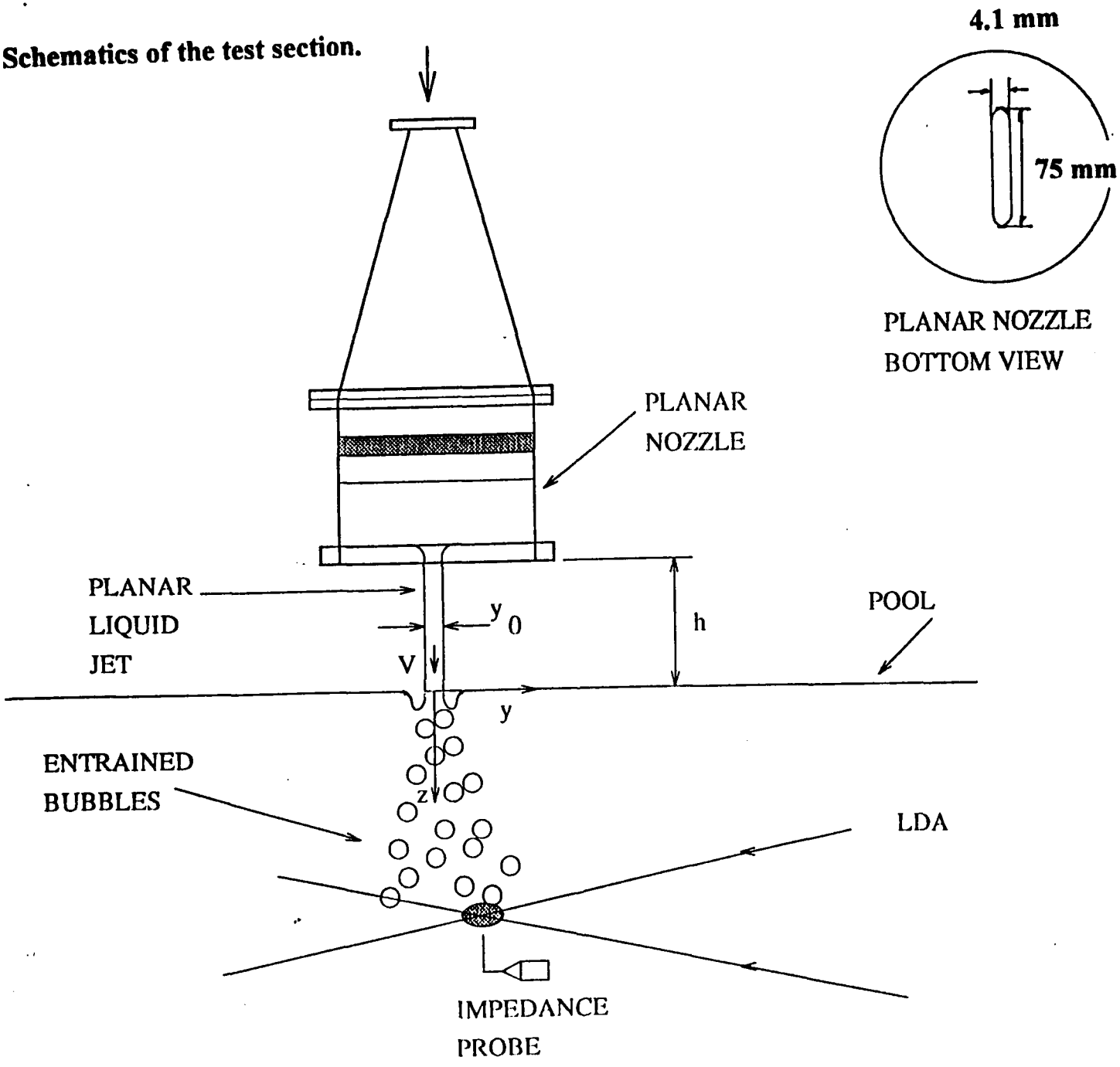

**Figure-2:Probability density function of the liquid axial velocity**

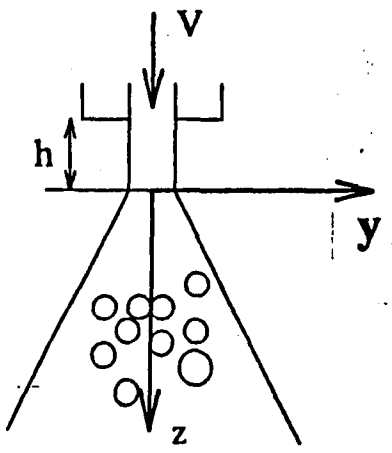


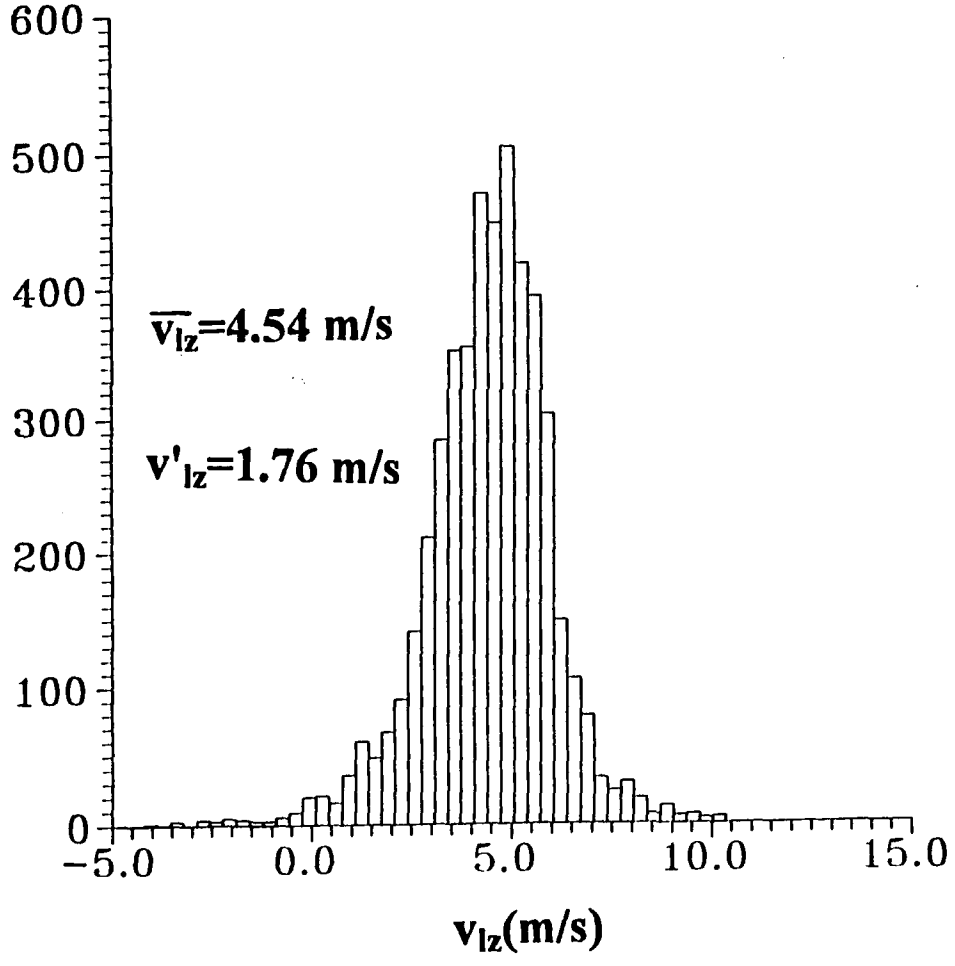


**w = 1.8 kg/s**

**h = 8.5 mm**

**z = 31 mm**

**Figure-3:Probability density function of the gas axial velocity**

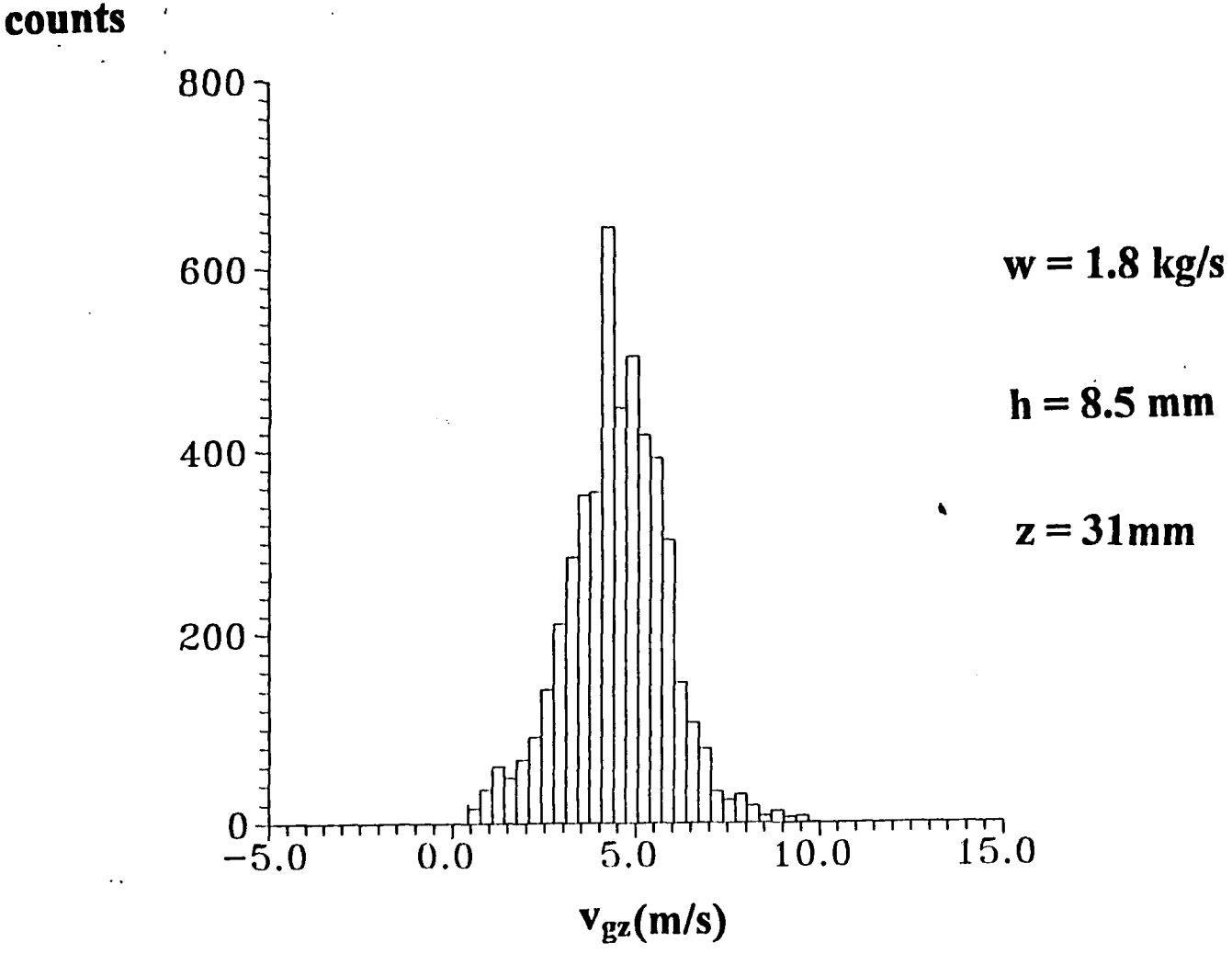

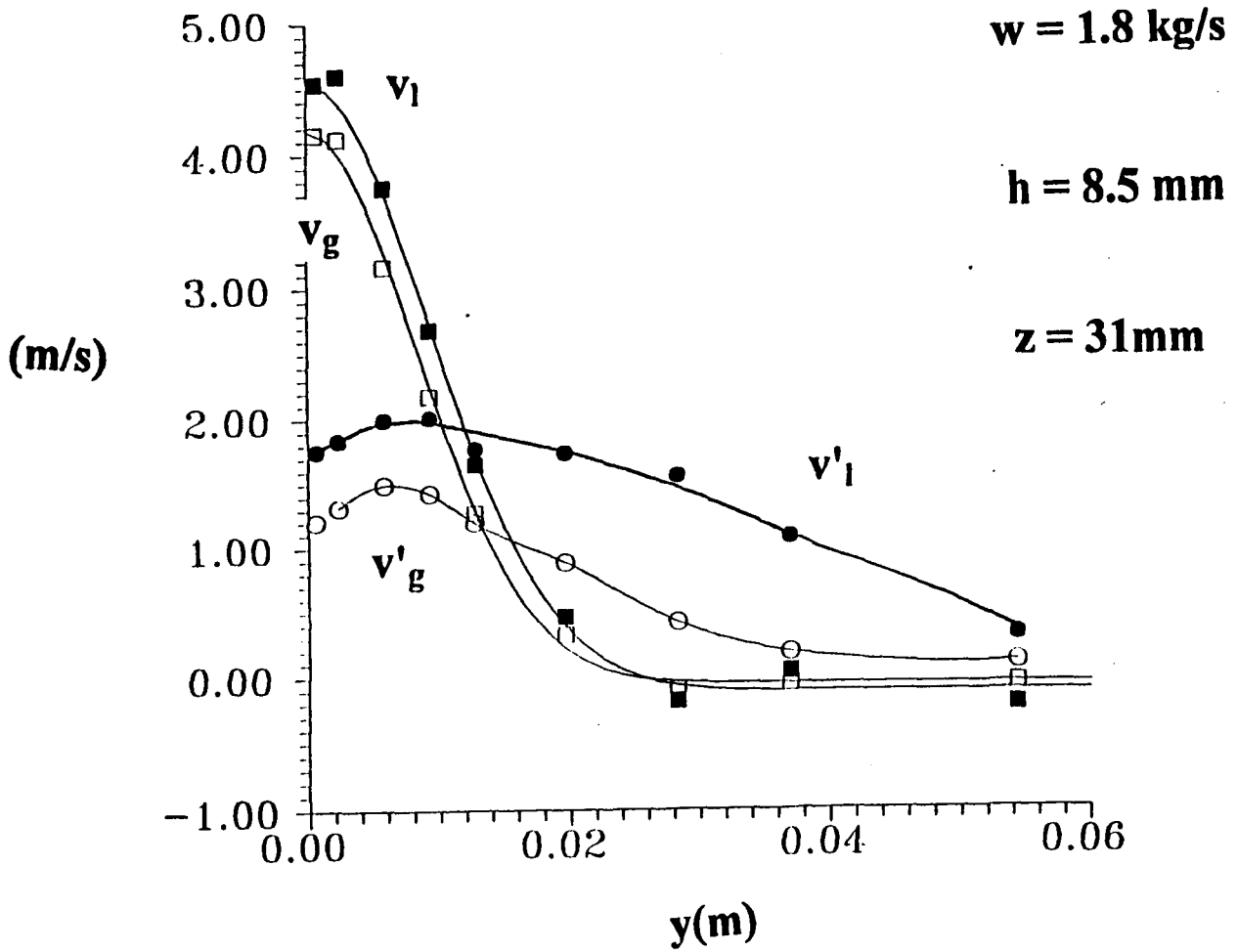


**Figure-4:Mean and rms axial velocities for the gas and liquid phases.**

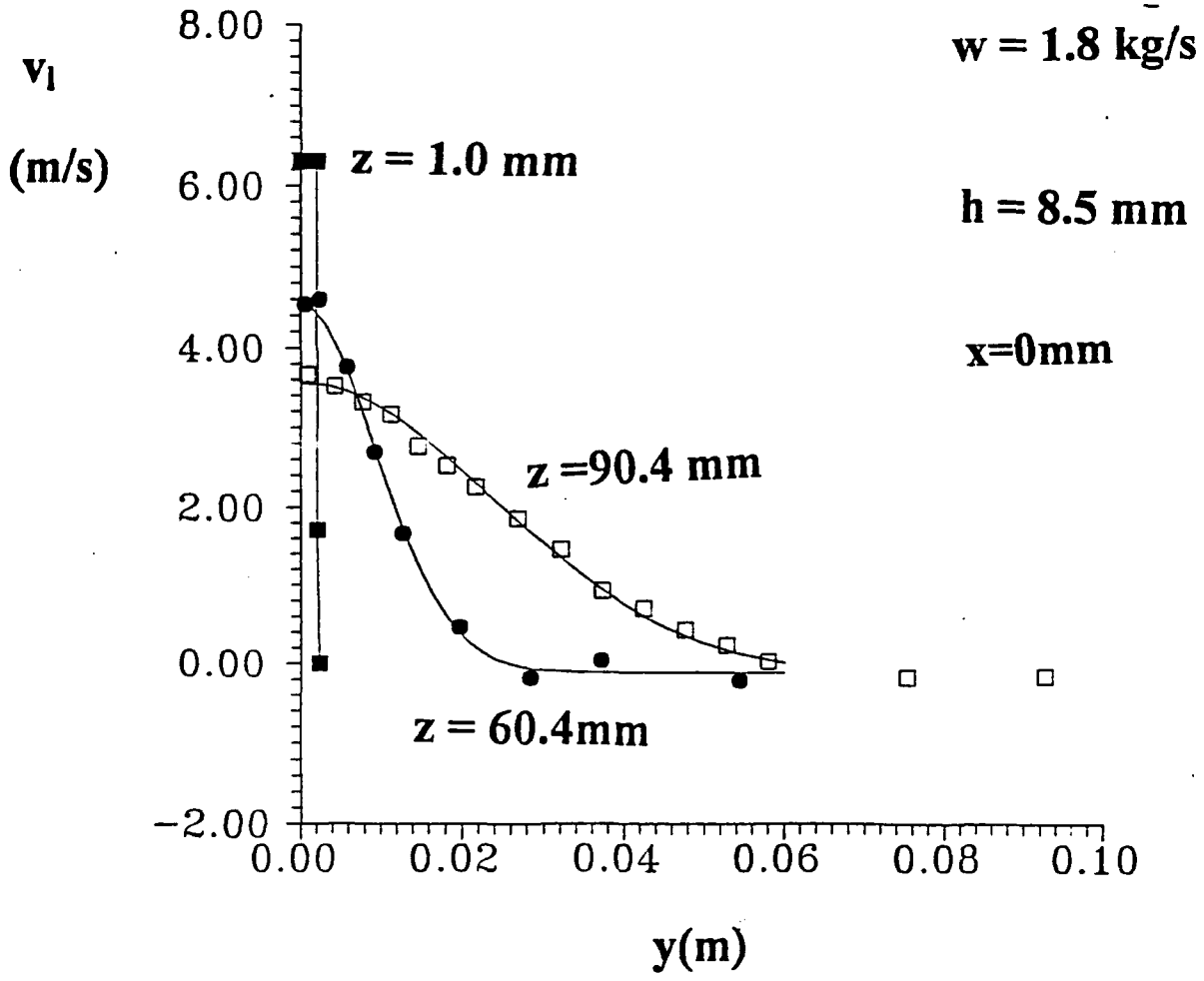


**Figure-5:Mean liquid axial velocities for different axial positions.**

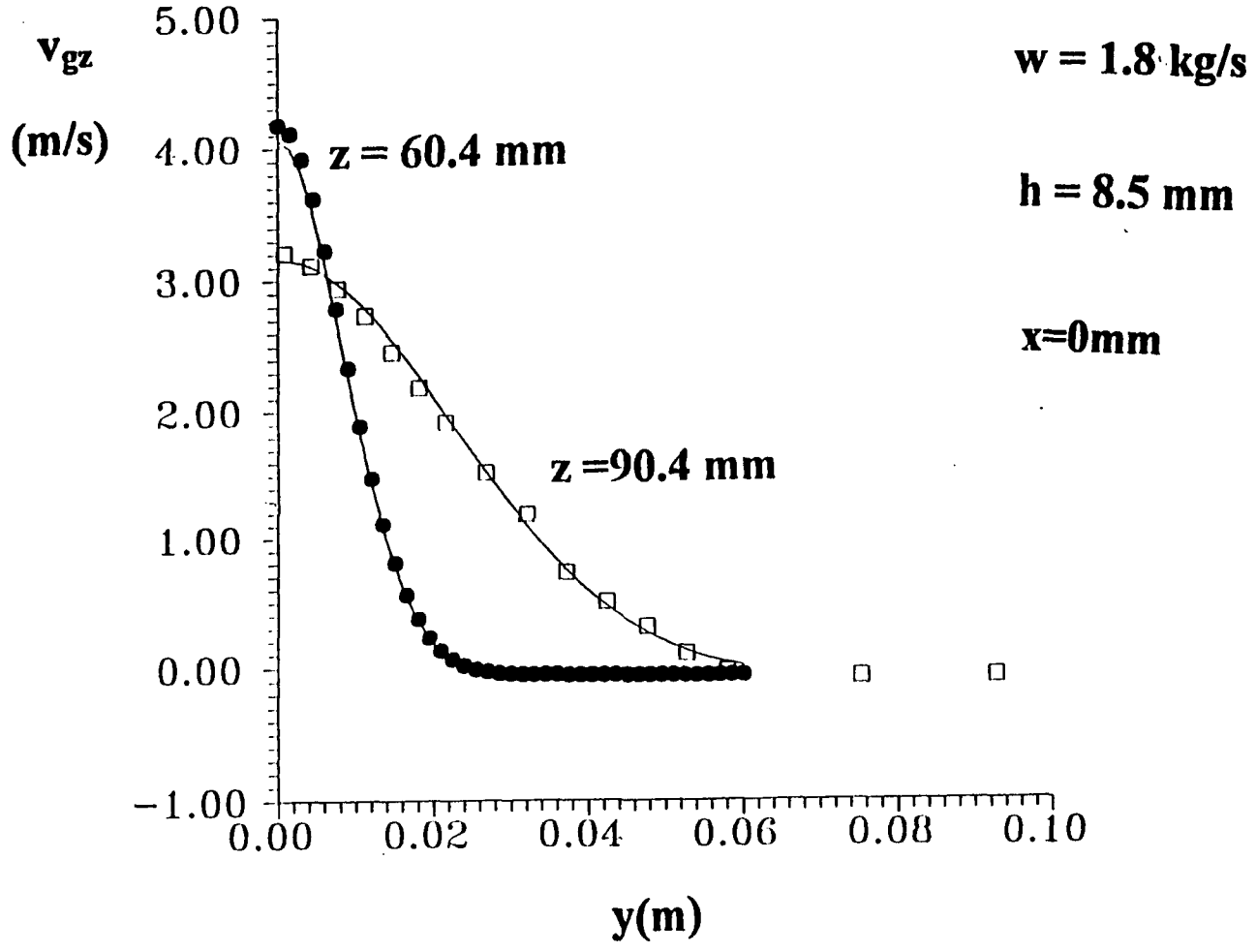


**Figure-6:Mean gas axial velocities for different axial positions.**

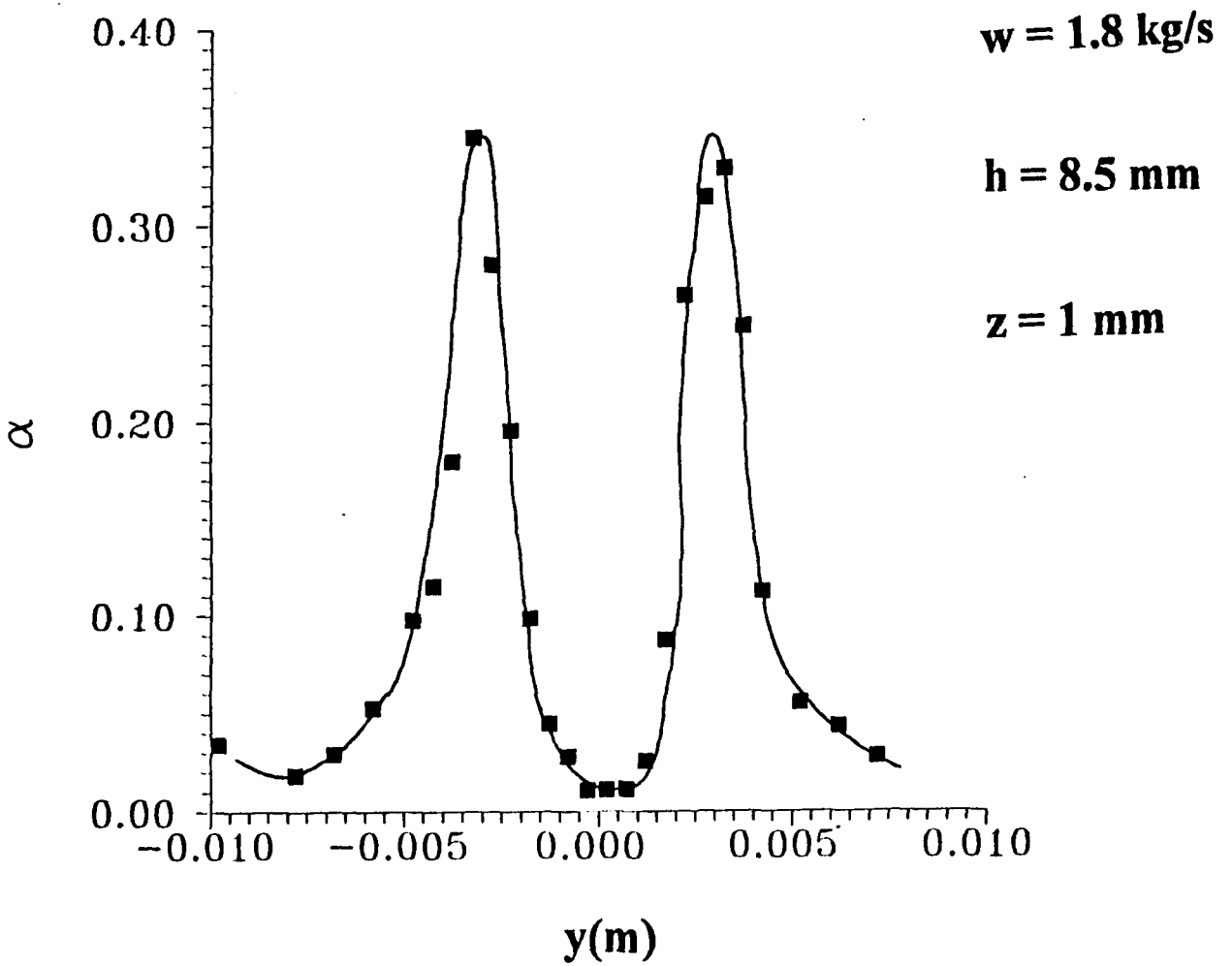


**Figure-7:Void fraction as a function of the lateral position.**

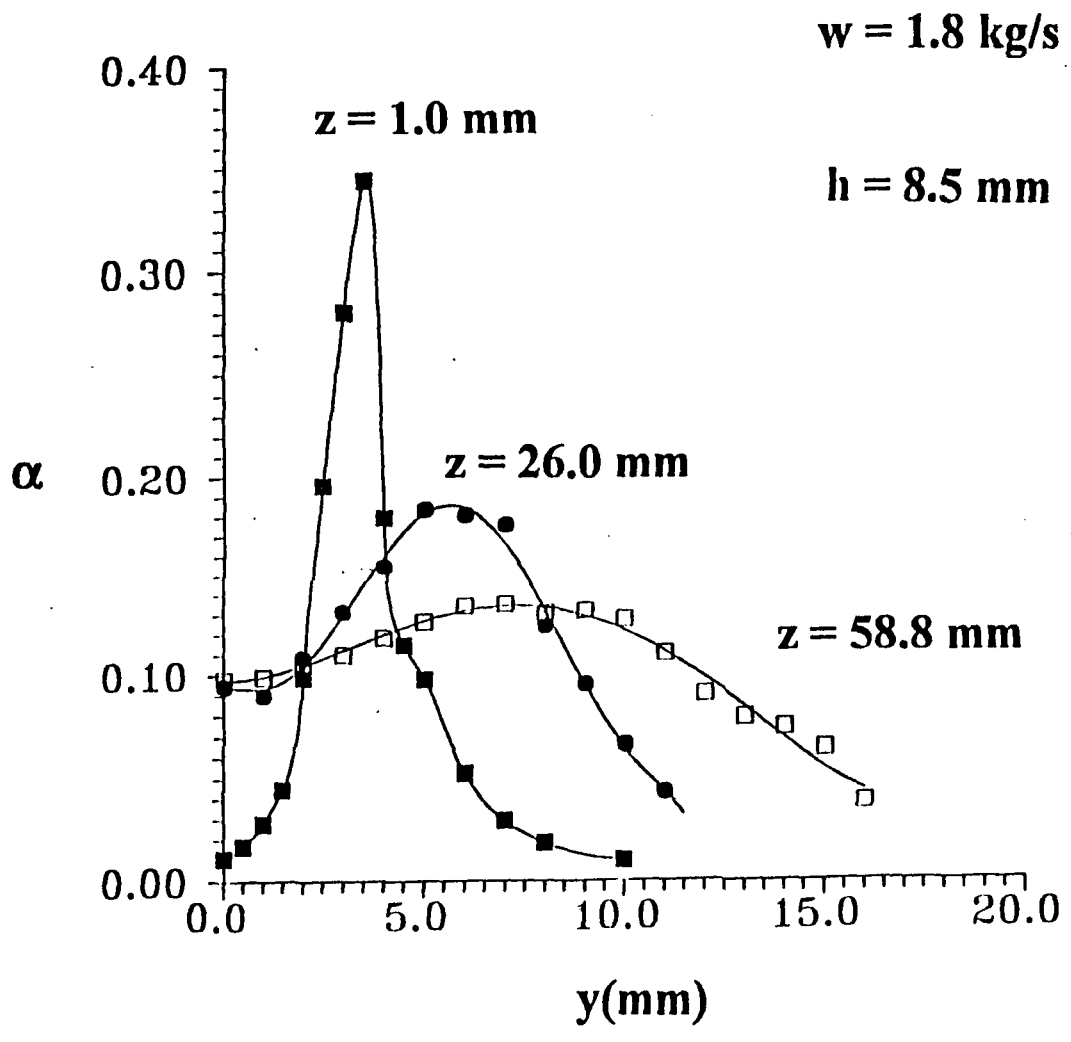


**Figure-8:Void fraction as a function of the lateral position for different axial positions.**

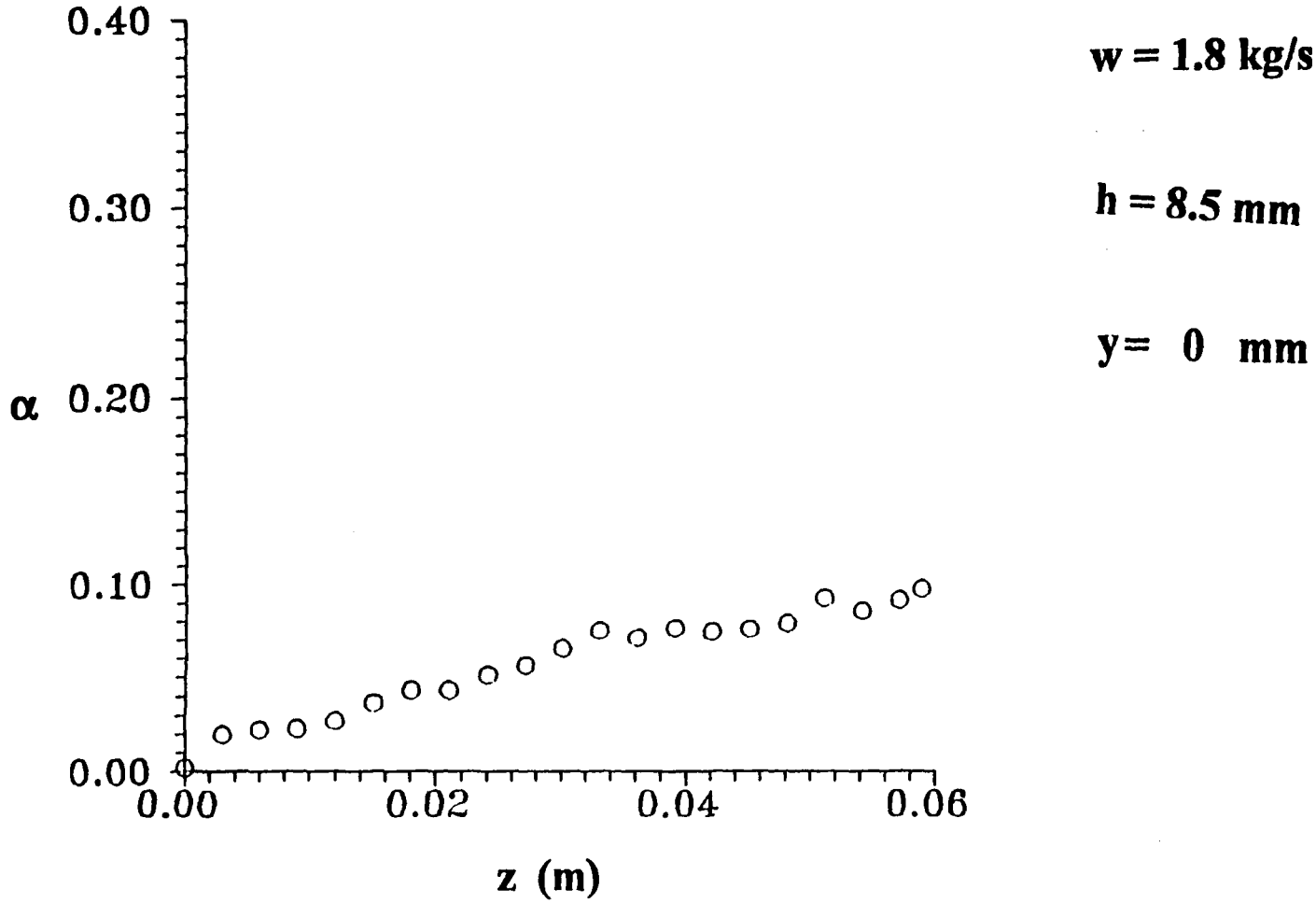


**Figure-9: Centerline void fraction as a function of the axial position.**